A high-performance optical lattice clock based on bosonic atoms

S. Origlia, M.S. Pramod, S. Schiller
Institut für Experimentalphysik, Heinrich-Heine-Universität Düsseldorf, 40225 Düsseldorf, Germany

Y. Singh, K. Bongs
University of Birmingham, Birmingham B15 2TT, United Kingdom

R. Schwarz, A. Al-Masoudi, S. Dörscher, S. Herbers, S. Häfner, U. Sterr and Ch. Lisdat
Physikalisch-Technische Bundesanstalt, 38116 Braunschweig, Germany

(Dated: February 24, 2018)

Optical lattice clocks with uncertainty and instability in the 10^{-17}-range and below have so far been demonstrated exclusively using fermions. Here, we demonstrate a bosonic optical lattice clock with 3×10^{-18} instability and 2.0×10^{-17} accuracy, both values improving on previous work by a factor 30. This was enabled by probing the clock transition with an ultra-long interrogation time of 4 s, using the long coherence time provided by a cryogenic silicon resonator, by careful stabilization of relevant operating parameters, and by operating at low atom density. This work demonstrates that bosonic clocks, in combination with highly coherent interrogation lasers, are suitable for high-accuracy applications with particular requirements, such as high reliability, transportability, operation in space, or suitability for particular fundamental physics topics. As an example, we determine the ^{88}Sr – ^{87}Sr isotope shift with 12 mHz uncertainty.

I. INTRODUCTION

Lattice optical clocks [1] have made strong progress in the past decade, both in terms of accuracy and stability. Atomic species intensely investigated so far are strontium, ytterbium, mercury, and magnesium. Best performances today include instability at low-10^{-16} level at $\tau = 1\,\mathrm{s}$ integration time [2–4], with the lowest value of $6 \times 10^{-17}/\sqrt{\tau/\mathrm{s}}$ achieved with dead-time-free interleaved interrogation of two atomic ensembles [5]. The lowest uncertainty has been estimated for an individual Sr clock, 2.1×10^{-18} [6], while direct lattice clock comparisons have achieved agreement with a fractional uncertainty of 4.4×10^{-18} at best [7]. Lattice clocks operated in different metrological institutes have been compared over long-distance links [8–11] and the feasibility of using lattice clocks for the realization of time scales has been demonstrated [12, 13]. First applications have also been reported: a transportable Sr lattice clock [14] has successfully completed measurement campaigns away from its home base [15]. Relativistic geodesy with uncertainty at the 5 cm-level has been implemented by comparing two clocks in different laboratories at 15 km distance [9]. A strontium lattice clock is also foreseen for the "Space Optical Clock on the ISS" mission of ESA [16].

Lattice clocks can be operated with bosonic or fermionic isotopes. Bosons exhibit some disadvantages compared with fermions, which has significantly slowed down their use for metrological applications: (i) the presence of s-wave collisions [17], which for spin-polarized fermions are suppressed, and which cause a significant frequency shift if uncontrolled, and (ii) a completely forbidden transition between the $^1\mathrm{S}_0$ and the $^3\mathrm{P}_0$ clock states, which requires the application of one or more additional external fields to enable driving the transition [18, 19]. These fields also cause a significant frequency shift [18–21]. On the other hand, the lifetime of the upper level is significantly shorter in fermions than in the bosonic isotopes, a fact that will become a limitation once the next generation of ultrastable lasers [22] is employed.

Turning to the specific case of strontium, the isotopes used so far are ^{87}Sr (fermion) and ^{88}Sr (boson). The bosonic isotope is attractive for realizing a simplified lattice clock, e.g. for transportation or for use in space on a satellite, where robustness and reliability are essential. Compared with ^{87}Sr, the atom cooling and clock spectroscopy are conceptually and technically simpler, thanks to the higher natural isotopic abundance (83% for ^{88}Sr versus 7% for ^{87}Sr) and absence of hyperfine structure [1, 23]. Furthermore, the Stark shift cancellation wavelength ("magic" lattice wavelength) in the bosonic isotope is basically insensitive to changes of the external magnetic field or of the lattice polarization axis [24]. It is also important to develop Sr bosonic clocks further in view of the fact that isotope shifts of all bosonic Sr atoms (^{84}Sr, ^{86}Sr, ^{88}Sr, ^{90}Sr) are of significant interest for the search of physics beyond the standard model [25]. In this context, a highly accurate measurement of the ^{88}Sr–^{87}Sr isotope shift has been recently performed in a dedicated setup, sharing large common-mode perturbations [21].

Although the potential of bosonic lattice clocks had been foreseen a long time ago [18], no experimental proof could be given, so far. In this paper, we demonstrate that a high-performance lattice clock is indeed feasible with a bosonic isotope.

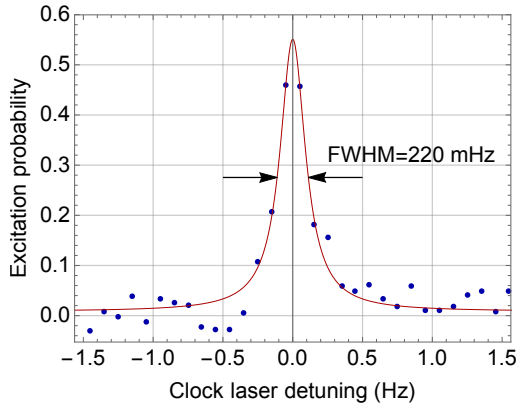

FIG. 1. Typical ^{88}Sr clock transition line for $T_\pi = 4.0$ s, bias field $B_{\mathrm{exp},0} \approx 0.21$ mT, clock laser intensity $I_{\mathrm{exp},0} \approx 28$ mW/cm^2. The line is a single scan (i.e., no averaging), with a total scan time of 165 s. The red line represents a Lorentzian fit with 220 mHz full width at half maximum (FWHM) linewidth.

II. MAGNETICALLY INDUCED SPECTROSCOPY

The optical excitation of the ^{1}S$_0$-^{3}P$_0$ clock transition in a bosonic atom can be enabled applying a bias magnetic field B. This results in a Rabi frequency for the interrogation of the clock transition given by $\Omega_{\mathrm{R}}/2\pi = \alpha\sqrt{I}\,|B|$, with the coupling coefficient $\alpha = 198\,\mathrm{Hz/T}\sqrt{\mathrm{mW/cm^2}}$ for ^{88}Sr [18] and the clock interrogation wave intensity I. For typical B-fields, I is 2 to 3 orders of magnitude stronger compared to fermionic lattice clocks [18]. The intensity leads to a probe light shift $\Delta\nu_{\mathrm{L}} = k\,I$, with $k = -18$ mHz/(mW/cm^2) [18], while the magnetic field leads to a 2$^{\mathrm{nd}}$-order Zeeman shift $\Delta\nu_{\mathrm{B}} = \beta\,B^2$, with $\beta = -23.8(3)$ MHz/T^2 [18]. Thus the Rabi frequency is proportional to $\sqrt{\Delta\nu_{\mathrm{L}} \cdot \Delta\nu_{\mathrm{B}}}$. The clock transition interrogation time, in case of Rabi spectroscopy, can be expressed as $T_\pi = \pi/\Omega_R$: therefore, the Rabi frequency, and consequently $\Delta\nu_L$ and $\Delta\nu_B$, can be reduced using a clock laser that supports longer T_π. The two shifts and the interrogation time are related by $|\Delta\nu_{\mathrm{L}}\Delta\nu_{\mathrm{B}}| = 2.8\,T_\pi^{-2}$. By choosing B and I appropriately, the minimum realizable shift magnitude is $|\Delta\nu_{\mathrm{L}} + \Delta\nu_{\mathrm{B}}|_{\mathrm{min}} = 3.3/T_\pi$. Furthermore, a long interrogation time reduces the effect of detection noise (including quantum projection noise) on the clock instability since these contributions scale as $1/\sqrt{T_\pi}$. As a consequence, operating the clock with low atom number with moderate degradation of the stability becomes possible.

III. THE EXPERIMENTAL APPARATUS

The lattice clock apparatus with its cooling and manipulation lasers is described in [26, 27]. Atoms are cooled and trapped in a 1D vertically oriented optical lattice (magic wavelength: 813 nm, $\sim 40\,\mu$m waist radius). The lifetime of the atoms in the lattice is >5 s. The clock laser (698 nm) is pre-stabilized on a 10 cm long transportable cavity [28] and phase-locked to a stationary clock laser stabilized on a 48 cm long reference cavity [29]. For most of the measurements, the latter was phase-locked, using a transfer-lock scheme [30], to a 1540 nm laser locked to a cryogenic silicon resonator [22], which exhibits less than 10 mHz linewidth and 4×10^{-17} instability at 1 s integration time. The clock laser radiation is delivered to the atoms via a phase-noise-cancelled optical fiber [31]. The clock laser waist radius is approximately 105 μm and provides a fairly homogeneous intensity profile across the atomic sample.

IV. SPECTROSCOPY AND CLOCK INSTABILITY

We investigated atom interrogation times up to $T_\pi = 8$ s. $T_\pi = 4$ s ($\Omega_{\mathrm{R}}/2\pi = 0.125$ Hz) was chosen as optimum value, the longest for which reliable Fourier-limited clock transition linewidths were observed (Fig. 1). This leads to a total cycle time of 5.3 to 6.3 s depending on the operating conditions. The observed linewidth of 0.22 Hz is in agreement with the theoretically expected value $0.8/T_\pi \simeq 0.2$ Hz [32]. The reason for the limited contrast (∼60%) can be attributed to collisional effects (see Section V E).

In order to control the probe light shift and Zeeman shift below the 1×10^{-17} (4.3 mHz) level, the clock laser beam power and the current $I_{\mathrm{B},0}$ in the bias field coils are actively stabilized. For the clock laser power we used a combination of an analog and digital power stabilization, acting on the RF power feeding an acousto-optic frequency shifter (AOM) in the clock laser breadboard. The digital stabilization serves as integrator of the analog error signal spanning several experimental cycles. It minimizes lock errors of the analog servo when the beam is turned on. With this system we can achieve a long-term beam power fractional instability below 1×10^{-3} over a few days, corresponding to $< 2 \times 10^{-18}$ for the fractional shift, for our interrogation parameters (see below). The current stabilization is based on a digital multimeter (DMM) measuring the current; the DMM reading is fed into a digital PID control, which steers the external control voltage of the power supply once every clock cycle. Based on the DMM's specifications, the expected fractional instability of the 2$^{\mathrm{nd}}$-order Zeeman shift, using $T_\pi = 4$ s and $I_{\mathrm{B},0} = +215$ mA, is below 2×10^{-4} (over 24 hours), corresponding to a 3.1×10^{-18} uncertainty on the frequency shift.

Any practical combination of clock laser intensity and bias field strength matching the desired Rabi frequency can be used. Based on the performance of the clock laser

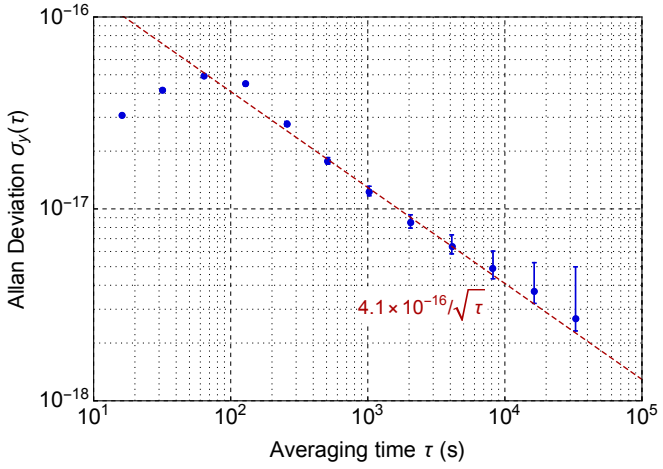

FIG. 2. Allan deviation of the fractional frequency offset between the ^{88}Sr clock and the PTB ^{87}Sr clock

power and bias field current stabilizations, we chose a clock laser intensity $I_{\mathrm{exp},0} \approx 28$ mW/cm^2 and a bias field $B_{\mathrm{exp},0} \approx 0.21$ mT, leading to shifts $\Delta\nu_{\mathrm{L},0} = k\, I_{\mathrm{exp},0} \approx -0.50$ Hz (5.8×10^{-16} in fractional units) and $\Delta\nu_{B,0} = \beta\, B^2_{\mathrm{exp},0} \approx -1.03$ Hz (2.4×10^{-15}).

In order to determine the clock instability, the bosonic clock was compared to the fermionic ^{87}Sr clock at PTB [4, 13]. Although the clock lasers of both clocks are prestabilized to the same cryogenic silicon cavity, on long time scales ($\tau > 200$ s), they are steered to the respective atomic references and, thus, independent. The combined instability is $4.1 \times 10^{-16}/\sqrt{\tau/\mathrm{s}}$, and averages down to the 3×10^{-18} level (Fig. 2). A number of measurements were acquired over the time span of a few months with similar results.

V. SYSTEMATIC SHIFT EVALUATION

Table I summarizes the uncertainty budgets of the bosonic and fermionic clock [33]. The systematic shifts of the bosonic clock were controlled and determined in the following way.

A. Blackbody radiation shift

For the evaluation of the blackbody radiation (BBR) shift, the temperature of the chamber is monitored by 17 temperature sensors (10 of them on the chamber windows). Thanks to the small size of the chamber (outer size $50 \times 50 \times 20$ mm^3) and of the MOT coils, a passive cooling system based on heat pipes is sufficient for dissipating most of the heat (about 8 W) produced by the MOT coils. We do not use any active temperature stabilization, but rely on the high stability of the laboratory temperature. The resulting difference between

	^{88}Sr clock		^{87}Sr clock	
Effect	$\Delta\nu$	u	$\Delta\nu$	u
BBR shift	523.2	0.8	492.2	1.5
BBR oven	0	0	0.9	0.9
Lattice shifts	2.2	1.1	0.9	0.4
Probe light shift ($\Delta\nu_{\mathrm{L}}$)	96.1	1.3	0.0	0.0
Cold collisions ($\Delta\nu_{\mathrm{LP}}$)	0.6	0.3	0.0	0.2
2$^{\mathrm{nd}}$-order Zeeman shift ($\Delta\nu_{\mathrm{B}}$)	209.7	0.5	3.4	0.1
Tunneling	0	0	0.0	0.3
Background gas collisions	0.13	0.13	0.8	0.8
DC-Stark shift	0.2	0.2	0.2	0.1
Total	827.1	2.0	498.4	2.0

TABLE I. Uncertainty budget for the ^{88}Sr and ^{87}Sr clocks. All numbers are expressed in parts per 10^{17}.

the warmest (T_{max}) and coldest point (T_{min}) of the vacuum chamber is between 250 and 400 mK, depending on operational parameters. Assuming a uniform probability distribution for the temperature experienced by the atoms, the mean temperature is $T_{\mathrm{avg}} = (T_{\mathrm{max}} + T_{\mathrm{min}})/2$ with uncertainty $(T_{\mathrm{max}} - T_{\mathrm{min}})/\sqrt{12}$ [34]. The BBR shift is computed from [6, 35]. An atomic beam shutter upstream from the atom chamber is closed during the atom interrogation cycle and shields the atoms from oven BBR.

B. Lattice light shift

For the lattice light shift evaluation we used the expression given in Katori *et al.* [36]:

$$\Delta\nu_{\mathrm{l}} = \zeta\left(n+\frac{1}{2}\right)\left(\frac{U_0}{E_{\mathrm{r}}}\right)^{1/2} +$$

$$-\left(\frac{\partial\Delta\alpha^{\mathrm{E1}}}{\partial\nu}\Delta\nu_{\mathrm{lat,m}} + \frac{3}{4}\Delta k_{\mathrm{H}}(2n^2+2n+1)\right)\frac{U_0}{E_{\mathrm{r}}} +$$

$$+\Delta k_{\mathrm{H}}(2n+1)\left(\frac{U_0}{E_{\mathrm{r}}}\right)^{3/2} - \Delta k_{\mathrm{H}}\left(\frac{U_0}{E_{\mathrm{r}}}\right)^2, \qquad (1)$$

where $\zeta = (\frac{\partial\Delta\alpha^{\mathrm{E1}}}{\partial\nu}\Delta\nu_{\mathrm{lat,m}} - \Delta\alpha^{\mathrm{E2,M1}})$, with $\Delta\alpha^{\mathrm{E1}} = \alpha_{\mathrm{e}}^{\mathrm{E1}} - \alpha_{\mathrm{g}}^{\mathrm{E1}}$ differential dipole polarizability, ν_{lat} lattice frequency, $\Delta\nu_{\mathrm{lat,m}}$ detuning of the lattice frequency from the magic value, and $\Delta\alpha^{\mathrm{E2,M1}} = (\alpha_{\mathrm{e}}^{\mathrm{E2}} + \alpha_{\mathrm{e}}^{\mathrm{M1}}) - (\alpha_{\mathrm{g}}^{\mathrm{E2}} + \alpha_{\mathrm{g}}^{\mathrm{M1}}) = 0.0(3)$ mHz [24] differential multipolar polarizability. The partial derivative of the differential dipole polarizability is given by $\frac{\partial\Delta\alpha^{\mathrm{E1}}}{\partial\nu_{\mathrm{lat}}} = 19.3 \times 10^{-12}$ (Hz Hz^{-1}) [36], n is the average motional state occupation, U_0 is the trap depth, and $E_{\mathrm{r}} = \hbar k_{\mathrm{lat}}^2/(2\pi)$ is the recoil energy, with k_{lat} the lattice wavenumber. Δk_{H} is the hyperpolarizability coefficient, whose most accurate

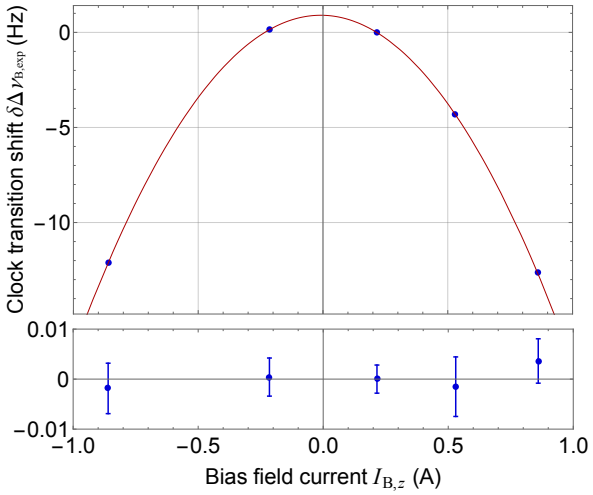

FIG. 3. Measurement of the 2nd-order Zeeman shift, and fit residuals, relative to the frequency shift at the operating point $I_{B,0} = +215$ mA, which is $\Delta\nu_{B,exp,0} = 898.9(29)$ mHz.

published value is 0.45(10) μHz/E_r^2 [37]. The bosonic isotope is not affected by tensor or vector shifts, due to the absence of a hyperfine structure.

The lattice light shift is measured by an interleaved clock operation at two different lattice depths, 100 E_r (shallow lattice) and 157 E_r (deep lattice), E_r being the lattice photon recoil energy. The difference in the transition frequency is thereby measured with a fractional uncertainty of 6.5×10^{-18}, after ~ 10000 s of averaging. This provides the detuning from the magic wavelength, solving Equation (1) for $\Delta\nu_{lat,m}$, which turned out to be 11 MHz. Sideband spectroscopy was used to evaluate the parameter n (1.4) and the lattice depth U_0 (129 E_r) under operating conditions. All the other parameters are known. The lattice shift is than evaluated for U_0 and is reported in Tab. I.

C. 2nd-order Zeeman shift

Fig. 3 shows the measurement of the 2nd-order Zeeman shift induced by the coupling field B (parallel to the lattice polarization axis, z-axis). Each point is acquired from an interleaved measurement, with two different currents $I_{ref,z}$ (reference current) and $I_{B,z}$. A system of switches allows inverting the current in the coils. The interrogation time T_π is set to match the different Rabi frequencies of the cycles. The data are fit with the function $\delta\Delta\nu_{B,exp} = \gamma((I_{ref,z} - I_{0,z})^2 - (I_{B,z} - I_{0,z})^2)$, where $I_{0,z}$ is the current necessary in order to compensate for the external offset field in z direction (maximum of the parabola). This gives $I_{0,z} = -0.009(2)$ A and $\gamma = 17.94(1)$ Hz/A^2: thus the shift at the reference current is $\Delta\nu_{B,exp,0} = \gamma(I_{0,z} - I_{ref,z})^2 = -900.2(22)$ mHz (see Tab. I).

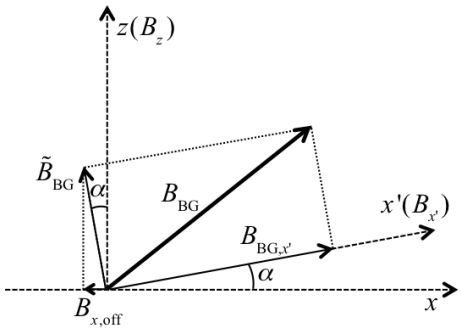

FIG. 4. Schematic of the magnetic field components for the 2nd-order Zeeman shift measurement. Details are given in the text.

Before measuring the shift induced by the field in the z-axis, we compensate for the offset fields in the x and y-axes. This is done by repeating the 2nd order Zeeman shift measurement, using two pairs of compensation coils with axes perpendicular to B, and finally setting their currents at the values which minimized the shift. It is important that the compensation of the perpendicular magnetic fields is done before the measurement of the shift induced by the coupling field B: in fact, in case the field produced by the compensation coils at the atom position is not perfectly perpendicular to B, a change of the current in the x and y compensation coils would result in a change of the offset field in the z direction (and, consequently, of the parameter $I_{0,z}$ in the fit function).

The same circumstance introduces an additional issue which is depicted in Fig. 4. B_{BG} is the background offset field, and x' is the direction of the field $B_{x'}$ produced by the x-compensation coils. x' is misaligned by an angle α from the x-direction. By minimizing the 2nd-order Zeeman shift as a function of the field produced by x-compensation coils, only the component $B_{BG,x'}$ of the background field is nulled. The remaining component $B_{BG,z'}$ introduces a residual offset field $B_{off,x}$ along the x-axis, which results in a residual shift. In order to estimate $B_{off,x}$, we evaluate the angle α. For this purpose we determine $B_{off,z}$ as function of $B_{x'}$. This is done by measuring the quadratic Zeeman shift for two opposite values of B (bias field in z-direction) and for $B_{x'} = 0$ and $B_{x'} = B_{x',max}$. We obtain $B_{off,x} = B_{off,z}/\tan\alpha$ and, from that, the residual shift. The same is repeated for the y-direction. In both cases, the residual shift is much smaller than 1×10^{-18}. If these remaining shifts were larger, they could be further reduced by iteration of the compensation procedure.

D. Probe light shift

Similarly, the probe light shift is measured (Fig. 5). The π-pulse condition is again fulfilled, for changing Rabi

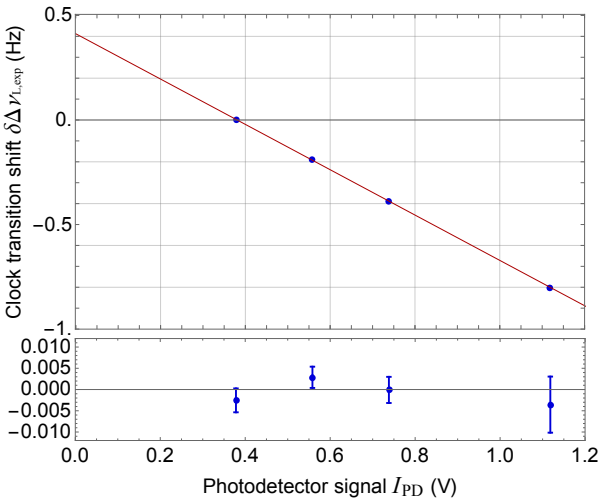

FIG. 5. Measurement of the probe light shift and fit residuals, relative to the shift at the operating point $I_{PD,0} = 378$ mV.

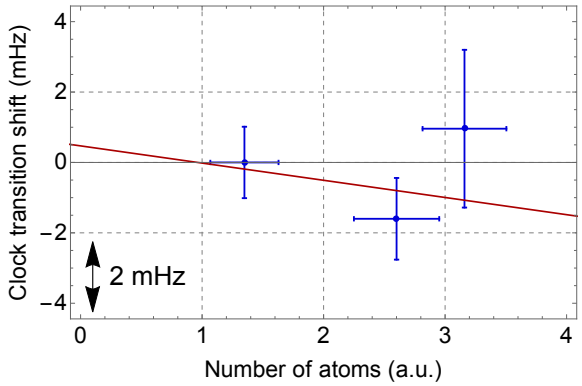

FIG. 6. Determination of the collisional shift. The standard deviation is used for the uncertainty on the atom number.

frequency due to intensity variation, by adapting T_π. The data are fit with a linear function. At the operating value, the measurement yields a shift $\Delta\nu_{L,exp,0} = -413.0(53)$ mHz. The difference compared with the expected shift of -0.50 Hz is attributed to the uncertainty of the intensity stabilization photodetector's calibration, and to non-perfect overlap between the clock and the lattice beam.

E. Cold collisional shift

1. *"Standard" determination*

For the evaluation of the density (cold collision) shift, we performed at first a "standard" measurement, varying the number of atoms trapped in the lattice by changing the Zeeman slower beam power. Due to the line broadening occurring at higher atomic densities (see next section), it is not possible to significantly increase the atom number compared to the operating value. This limits the range of data available for the shift determination. The measurement is performed by running the clock with a single atomic servo (i.e., not in interleaved mode) and using the PTB Sr clock as flywheel. Fig. 6 shows the result. During the measurement at the lowest atom number (left-most data point) the number of atoms is actively stabilized, by correcting appropriately the 461 nm slower wave power. From a fit to the data the cold collisional shift for the atom number under operating conditions is 0.5(22) mHz ($1(5) \times 10^{-18}$).

2. *Alternative evaluation: lineshape analysis*

In addition to the "standard" determination, we introduce a novel approach based on a lineshape analysis. Fig. 7 shows two clock transition scans obtained with $T_\pi = 1.0$ s interrogation time. Following the works presented in [38, 39], which report the observation of atomic interaction sidebands by proper control of interaction parameters, we model the lineshape as a sum of two Lorentzian profiles: the main one (green) results from the atoms in singly-occupied lattice sites, its width is close to the Fourier limit. The second profile (red) results from atoms in multiply occupied lattice sites. It has a broader width and a negative frequency shift [17]. In order to confirm this model, we used photoassociation (PA) [40]: two atoms in the same lattice site form an excited Sr_2 molecule by interacting with a photon from the PA beam. The molecule decays with high probability into two hot atoms, which are lost from the lattice. In this way, the fraction of multiply occupied sites is reduced. The PA transition is driven by a radiation detuned by about -222 MHz from the $^1S_0$-$^3P_1$ transition [21] (689 nm, obtained from the same laser as employed in the laser cooling) applied for 600 ms before the clock interrogation, with an intensity of about 1 W/cm^2. During the line scan in Fig. 7(a), the PA beam frequency is detuned by a few MHz from the PA transition. This ensures that all disturbances due to the PA beam (such as atom heating), except for the PA process itself, are equal to the situation in Fig. 7(b), where the PA laser is tuned on-resonance. The comparison between the two lineshapes confirms the model: the contribution of the profile from multiply occupied sites (red) is reduced when PA is applied. The fact that this contribution is not fully cancelled could be explained by excited molecules decaying into the internal ground-state and remaining trapped in sites that were originally occupied by three or more Sr atoms. These could than lead to collisional broadening and shifts. Having verified this model, we can assume that the main profile (green) represents the unperturbed transition (i.e., atoms not affected by collisions) and evaluate the collisional shift as the line pulling due to the

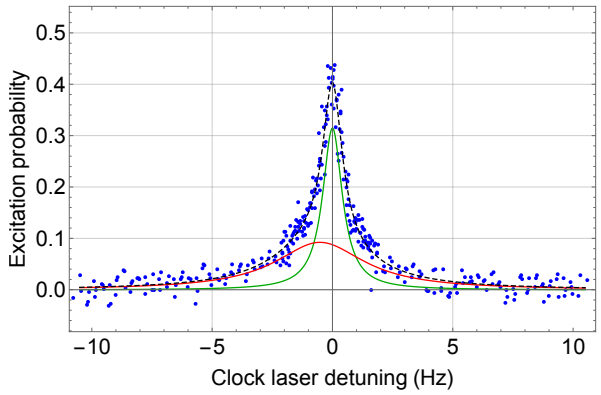

(a)

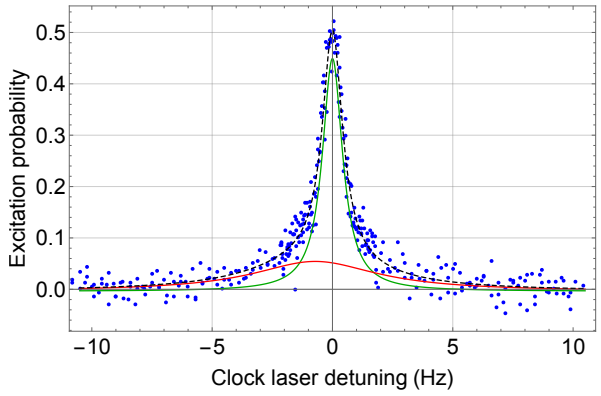

(b)

FIG. 7. Clock transition scans acquired with T_π =1.0 s interrogation time (a) with detuned photoassociation laser applied before each atom interrogation, (b) with resonant PA laser. The blue dashed curve is the fit function including a line from singly occupied sites (green) and a second line from multiply occupied sites (red). Details are given in the text.

second profile. Furthermore, in order to be less sensitive to this line pulling, the main profile interrogation is done experimentally at two detunings closer to the center of the main profile than at half height.

During the measurement of the isotope shift (see Section VI) no PA beam was used. However, the atoms were loaded into the lattice starting from a red MOT with higher temperature and larger size, meaning lower density, spreading the atoms over more lattice sites. In addition, the longer interrogation time provides narrower transition lines from singly occupied sites and reduces the effect of line pulling. The resulting line pulling during the measurement of the ^{88}Sr–^{87}Sr isotope shift is $\Delta\nu_{\mathrm{LP}} = 2.5(15)$ mHz, or $5.7(34) \times 10^{-18}$, consistent with the result obtained with "standard" evaluation, 0.5(22) mHz ($1(5) \times 10^{-18}$).

F. DC Stark shift

The DC Stark shift is a potential issue, since the small size of the vacuum chamber places the non-conductive chamber windows, a potential location of accumulated electric charges, as close as 7 mm to the atoms. The shift is measured by applying voltages, in turn, to three pairs of approximately circular wire electrodes placed externally to the windows, and measuring the resulting clock transition frequency shift. From the quadratic fit, the residual shift for the operating condition of zero applied voltages is $2(2) \times 10^{-18}$.

G. Background gas collisions shift

The background gas collisions shift can be evaluated, as reported in [41], from the lattice lifetime and using the coefficients given in [42]. The measured lattice lifetime is 5.6 s, leading to a shift of $-1.3(13) \times 10^{-18}$.

H. Tunneling

We assume the contribution of tunneling to be negligible, since the lattice beams are vertically oriented and the lattice is deep [43].

VI. ISOTOPE SHIFT MEASUREMENT

For the evaluation of the isotope shift, from the comparison with the PTB clock, we used the average of four measurements (Fig. 8) acquired over two days. The lattice shift, probe light shift and the Zeeman shift measure-

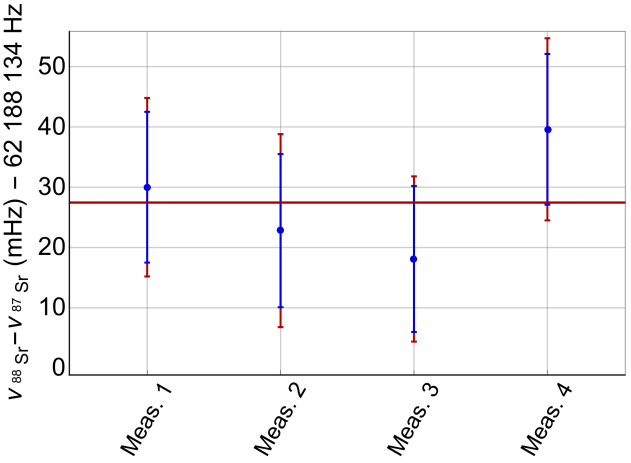

FIG. 8. Measurement used for the evaluation of the isotope shift value (red dashed line). The red and blue error bars represent the statistical and systematic uncertainty.

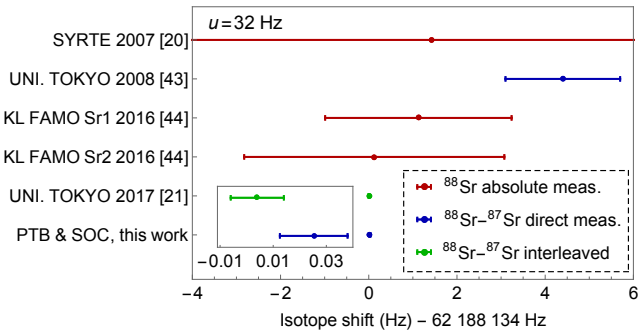

FIG. 9. Present isotope shift, compared with published values.

ments were acquired in the same days. The systematic uncertainty, 12 mHz, arises from the bosonic clock's uncertainty and the PTB clock's uncertainty, The resulting ^{88}Sr–^{87}Sr isotope shift is 62 188 134.027(12) Hz, where the uncertainty corresponds to 3.0×10^{-17}. In Fig. 9 our measurement is compared with previously published values. In particular, the difference compared with the value recently reported in [21] is within 2σ of the combined uncertainty of both measurements.

VII. CONCLUSIONS AND OUTLOOK

In conclusion, we have demonstrated a bosonic optical lattice clock with 3×10^{-18} instability and 2.0×10^{-17} inaccuracy. This result was obtained by operating the clock with long interrogation times of 4 s, with suitably low atom density, stabilizing the important physical parameters of the apparatus with active control, and accurate evaluation of the shifts. The long interrogation time was only possible by exploiting the ultra-low instability of a cryogenic reference cavity [22]. As a consequence, we determined the ^{88}Sr–^{87}Sr isotope shift with 12 mHz inaccuracy. With this study, we realize the long-predicted potential of bosonic lattice clocks, with a factor of approximately 30 improvement in terms of accuracy and instability compared with the best values reported so far [21].

We see significant potential for improving this approach further, by achieving a longer atom lifetime in the lattice, and implementing for instance higher-dimensional lattices, hyper-Ramsey spectroscopy [44] and PA. Bosonic clocks may than become competitive with fermionic ones, mainly for applications where simplicity, reliability, or fundamental physics are essential. The present technique could also be applied to other species (Yb, Mg), which have values of $|\Delta\nu_{\mathrm{L}} + \Delta\nu_{\mathrm{B}}|_{\mathrm{min}}$ similar to Sr [18].

The authors are very grateful to C. Klempt and I. Kruse from Leibniz-Universität Hannover for providing the control software for the FPGA, to D. Iwaschko and U. Rosowski (HHU), and to M. Misera, A. Koczwara and A. Uhde (PTB) for technical assistance and useful discussion, to T. Legero and D.G. Matei for making available the cryogenic silicon cavity, and to E. Benkler for operating the frequency comb. We are indebted to the members of the SOC2 consortium for their contributions to the early development of the apparatus described here and for equipment loan. We thank L. Cacciapuoti (ESA) for constant support. This work was funded in part by the FP7-MSCA-ITN project No. 607493 "FACT", the H2020-MSCA-RISE- project No. 691156 "Q-Sense" and ESA project No. 4000119716 ("I-SOC"). The PTB team acknowledges funds from the CRC 1227 DQ-mat within project B02.

[1] H. Katori, M. Takamoto, V. G. Pal'chikov, and V. D. Ovsiannikov, Phys. Rev. Lett. **91**, 173005 (2003).
[2] T. L. Nicholson, M. J. Martin, J. R. Williams, B. J. Bloom, M. Bishof, M. D. Swallows, S. L. Campbell, and J. Ye, Phys. Rev. Lett. **109**, 230801 (2012).
[3] N. Hinkley, J. A. Sherman, N. B. Phillips, M. Schioppo, N. D. Lemke, K. Beloy, M. Pizzocaro, C. W. Oates, and A. D. Ludlow, Science **341**, 1215 (2013).
[4] A. Al-Masoudi, S. Dörscher, S. Häfner, U. Sterr, and C. Lisdat, Phys. Rev. A **92**, 063814 (2015).
[5] M. Schioppo, R. C. Brown, W. F. McGrew, N. Hinkley, R. J. Fasano, K. Beloy, T. H. Yoon, G. Milani, D. Nicolodi, J. A. Sherman, N. B. Phillips, C. W. Oates, and A. D. Ludlow, Nat. Photonics **11**, 48 (2017).
[6] T. Nicholson, S. Campbell, R. Hutson, G. Marti, B. Bloom, R. McNally, W. Zhang, M. Barrett, M. Safronova, W. Strouse, G.F. Tew, and J. Ye, Nat. Comm. **6**, 6896 (2015).
[7] I. Ushijima, M. Takamoto, M. Das, T. Ohkubo, and H. Katori, Nat. Photonics **9**, 185 (2015).
[8] D. Calonico, E. K. Bertacco, C. E. Calosso, C. Clivati, G. A. Costanzo, M. Frittelli, A. Godone, A. Mura, N. Poli, D. V. Sutyrin, G. Tino, M. E. Zucco, and F. Levi, Appl. Phys. B **117**, 979 (2014).
[9] T. Takano, M. Takamoto, I. Ushijima, N. Ohmae, T. Akatsuka, A. Yamaguchi, Y. Kuroishi, H. Munekane, B. Miyahara, and H. Katori, Nat. Photonics **10**, 662 (2016).
[10] C. Lisdat, G. Grosche, N. Quintin, C. Shi, S. Raupach, C. Grebing, D. Nicolodi, F. Stefani, A. Al-Masoudi, S. Dörscher, S. Häfner, J.-L. Robyr, N. Chiodo, S. Bilicki, E. Bookjans, A. Koczwara, S. Koke, A. Kuhl, F. Wiotte, F. Meynadier, E. Camisard, M. Abgrall, M. Lours, T. Legero, H. Schnatz, U. Sterr, H. Denker, C. Chardonnet, Y. Le Coq, G. Santarelli, A. Amy-Klein, R. Le Targat, J. Lodewyck, O. Lopez, and P.-E. Pottie, Nat. Comm. **7**, 12443 (2016).
[11] K. Predehl, G. Grosche, S. M. F. Raupach, S. Droste, O. Terra, J. Alnis, T. Legero, T. W. Hänsch, T. Udem, R. Holzwarth, and H. Schnatz, Science **336**, 441 (2012).
[12] J. Lodewyck, S. Bilicki, E. Bookjans, J. L. Robyr, C. Shi, G. Vallet, R. Le Targat, D. Nicolodi, Y. Le Coq, and

J. Guéna, Metrologia **53** (2016).
[13] C. Grebing, A. Al-Masoudi, S. Dörscher, S. Häfner, V. Gerginov, S. Weyers, B. Lipphardt, F. Riehle, U. Sterr, and C. Lisdat, Optica **3**, 563 (2016).
[14] S. B. Koller, J. Grotti, S. Vogt, A. Al-Masoudi, S. Dörscher, S. Häfner, U. Sterr, and C. Lisdat, Phys. Rev. Lett. **118**, 073601 (2017).
[15] J. Grotti, S. Koller, S. Vogt, S. Häfner, U. Sterr, C. Lisdat, H. Denker, C. Voigt, L. Timmen, A. Rolland, F. N. Baynes, H. S. Margolis, M. Zampaolo, P. Thoumany, M. Pizzocaro, B. Rauf, F. Bregolin, A. Tampellini, P. Barbieri, M. Zucco, G. A. Costanzo, C. Clivati, F. Levi, and D. Calonico, Nature Physics (2018), 10.1038/s41567-017-0042-3.
[16] S. Schiller, A. Görlitz, A. Nevsky, S. Alighanbari, S. Vasilyev, C. Abou-Jaoudeh, G. Mura, T. Franzen, U. Sterr, S. Falke, C. Lisdat, E. Rasel, A. Kulosa, S. Bize, J. Lodewyck, G. M. Tino, N. Poli, M. Schioppo, K. Bongs, Y. Singh, P. Gill, G. Barwood, Y. Ovchinnikov, J. Stuhler, W. Kaenders, C. Braxmaier, R. Holzwarth, A. Donati, S. Lecomte, D. Calonico, F. Levi, and members of the SOC2 teams, Let's embrace space II **Ch. 45, 452–463** (2012).
[17] C. Lisdat, J. S. R. Vellore Winfred, T. Middelmann, F. Riehle, and U. Sterr, Phys. Rev. Lett. **103**, 090801 (2009).
[18] A. V. Taichenachev, V. I. Yudin, C. W. Oates, C. W. Hoyt, Z. W. Barber, and L. Hollberg, Phys. Rev. Lett. **96**, 083001 (2006).
[19] T. Hong, C. Cramer, W. Nagourney, and E. N. Fortson, Phys. Rev. Lett. **94**, 050801 (2005).
[20] X. Baillard, M. Fouché, R. Le Targat, P. G. Westergaard, A. Lecallier, Y. Le Coq, G. D. Rovera, S. Bize, and P. Lemonde, Opt. Lett. **32**, 1812 (2007).
[21] T. Takano, R. Mizushima, and H. Katori, Appl. Phys. Express **10**, 072801 (2017).
[22] D. G. Matei, T. Legero, S. Häfner, C. Grebing, R. Weyrich, W. Zhang, L. Sonderhouse, J. M. Robinson, J. Ye, F. Riehle, and U. Sterr, Phys. Rev. Lett. **118**, 263202 (2017).
[23] T. Mukaiyama, H. Katori, T. Ido, Y. Li, and M. Kuwata-Gonokami, Phys. Rev. Lett. **90**, 113002 (2003).
[24] P. G. Westergaard, J. Lodewyck, L. Lorini, A. Lecallier, E. A. Burt, M. Zawada, J. Millo, and P. Lemonde, Phys. Rev. Lett. **106**, 210801 (2011).
[25] C. Delaunay, R. Ozeri, G. Perez, and Y. Soreq, Phys. Rev. D **96**, 093001 (2017).
[26] K. Bongs, Y. Singh, L. Smith, W. He, O. Kock, D. Świerad, J. Hughes, S. Schiller, S. Alighanbari, S. Origlia, S. Vogt, U. Sterr, C. Lisdat, R. Le Targat, J. Lodewyck, D. Holleville, B. Venon, S. Bize, G. P. Barwood, P. Gill, I. R. Hill, Y. B. Ovchinnikov, N. Poli, G. M. Tino, J. Stuhler, and W. Kaenders, C. P. Phys. **16**, 553 (2015).
[27] S. Origlia, S. Schiller, M. Pramod, L. Smith, Y. Singh, W. He, S. Viswam, D. Świerad, J. Hughes, K. Bongs, U. Sterr, C. Lisdat, S. Vogt, S. Bize, J. Lodewyck, R. Le Targat, D. Holleville, B. Venon, P. Gill, G. Barwood, I. R. Hill, Y. Ovchinnikov, A. Kulosa, W. Ertmer, E. M. Rasel, J. Stuhler, and W. Kaenders, Proc. SPIE 9900, Quantum Optics, 990003 (April 29, 2016), doi: 10.1117/12.2229473.
[28] S. Vogt, C. Lisdat, T. Legero, U. Sterr, I. Ernsting, A. Nevsky, and S. Schiller, Appl. Phys. B **104**, 741 (2011).
[29] S. Häfner, S. Falke, C. Grebing, S. Vogt, T. Legero, M. Merimaa, C. Lisdat, and U. Sterr, Opt. Lett. **40**, 2112 (2015).
[30] J. Stenger, H. Schnatz, C. Tamm, and H. Telle, Phys. Rev. Lett. **88**, 073601 (2002).
[31] S. Falke, M. Misera, U. Sterr, and C. Lisdat, Appl. Phys. B **107**, 301 (2012).
[32] G. J. Dick, in *Proceedings of* 19^{th} *Annu. Precise Time and Time Interval Meeting, Redendo Beach, 1987* (U.S. Naval Observatory, Washington, DC, 1988) pp. 133–147.
[33] S. Falke, N. Lemke, C. Grebing, B. Lipphardt, S. Weyers, V. Gerginov, N. Huntemann, C. Hagemann, A. Al-Masoudi, S. Häfner, S. Vogt, U. Sterr, and C. Lisdat, New J. Phys **16** (2014).
[34] GUM, Guide to the Expression of Uncertainty in Measurement, ISO/TAG 4. (ISO, 1993) (corrected and reprinted, 1995) in the name of the BIPM, IEC, IFCC, ISO, UPAC, IUPAP, and OILM (Sèrres, France, 1995), ISBN 92-67-10188-9,1995.
[35] T. Middelmann, S. Falke, C. Lisdat, and U. Sterr, Phys. Rev. Lett. **109**, 263004 (2012).
[36] H. Katori, V. D. Ovsiannikov, S. I. Marmo, and V. G. Palchikov, Phys. Rev. A **91**, 052503 (2015).
[37] R. Le Targat, L. Lorini, Y. Le Coq, M. Zawada, J. Guéna, M. Abgrall, M. Gurov, P. Rosenbusch, D. G. Rovera, B. Nagórny, R. Gartman, P. Westergaard, M. Tobar, M. Lours, G. Santarelli, A. Clairon, S. Bize, P. Laurent, P. Lemonde, and J. Lodewyck, Nature Comm. **4**, 2109 (2013).
[38] M. Bishof, Y. Lin, M. D. Swallows, A. V. Gorshkov, J. Ye, and A. M. Rey, Phys. Rev. Lett. **106**, 250801 (2011).
[39] N. D. Lemke, J. von Stecher, J. A. Sherman, A. M. Rey, C. W. Oates, and A. D. Ludlow, Phys. Rev. Lett. **107**, 103902 (2011).
[40] T. Zelevinsky, M. M. Boyd, A. D. Ludlow, T. Ido, J. Ye, R. Ciuryło, P. Naidon, and J. P. S., Phys. Rev. Lett. **96**, 203201 (2006).
[41] K. Gibble, in *2013 Joint European Frequency and Time Forum International Frequency Control Symposium (EFTF/IFC)* (2013) pp. 46–47.
[42] J. Mitroy and J. Zhang, Mol. Phys. **108**, 1999 (2010), 10.1080/00268976.2010.501766.
[43] P. Lemonde and P. Wolf, Phys. Rev. A **72**, 033409 (2005).
[44] V. I. Yudin, A. V. Taichenachev, C. W. Oates, Z. W. Barber, N. D. Lemke, A. D. Ludlow, U. Sterr, C. Lisdat, and F. Riehle, Phys. Rev. A **82**, 011804(R) (2010).